RSC Advances

PAPER

View Article Online
View Journal | View Issue

Cite this: *RSC Adv.*, 2020, **10**, 39087

Mechanical behavior of SiNC layers on PDMS: effects of layer thickness, PDMS modulus, and SiNC surface functionality†

Alborz Izadi,‡ Mayank Sinha,‡ Cameron Papson, Sara Roccabianca and Rebecca Anthony *

Received 20th July 2020
Accepted 22nd September 2020

DOI: 10.1039/d0ra06321e

rsc.li/rsc-advances

Thin layers of nanomaterials on stretchable substrates have the potential to enable stretchable, bendable optoelectronic devices, wearable diagnostics, and more. Recently, our group reported on a novel method for finding the neo-Hookean coefficient of thin layers of silicon nanocrystals (SiNCs) on polydimethylsiloxane (PDMS). Here we elaborate on that initial study by examining the effects of the SiNC layer thickness, PDMS neo-Hookean coefficient, and SiNC surface functionality on the neo-Hookean coefficient of the SiNC layers. We found that, while the layer thickness and PDMS neo-Hookean coefficient influence the behavior of the SiNC layers, layers of surface-functionalized SiNCs do not exhibit disparate behavior from layers of bare SiNCs.

1 Introduction

In situ investigation of the mechanical properties of nanomaterials in the form of thin films is a challenging obstacle in the advancement of nanotechnology. Nanoindentation experiments and other physical probe-based techniques can be used to evaluate single-nanocrystal deformation in elastic and plastic regimes.[1–10] However, behavior of nanoparticle ensembles, particularly in layers on arbitrary substrates, is more difficult to elucidate *in situ*, as many of these methods are irreversible and/or destructive. Furthermore, the mechanical behavior of thin films of nanomaterials can also depend on the substrate's mechanical properties, emphasizing the importance of *in situ* measurement techniques. Thus, there is a significant interest in non-destructive methods for evaluating properties of thin films, especially for layers of nanoparticles on elastomeric substrates which can prohibit indentation-type methods. The future of electronics strongly relies on advancement in mechanical flexibility, sustainability and biocompatibility of electro-optical sensors, health monitoring systems, photovoltaic devices, displays, and functional coatings. Therefore, evaluating the mechanical behavior of these thin-film ensembles of nanoparticles is critical for robust device design.

Several attempts have been made to evaluate the mechanical properties of nanocrystalline materials deposited on a substrate. Different methods have been applied to evaluate properties in both the elastic[10–12] as well as the plastic regimes.[1,4,6–8,13] Employing instability, specifically has recently gained popularity towards becoming a viable manner to evaluate the mechanical properties of thin films deposited on soft substrates. Examples include evaluating the mechanical properties of thin films (5 nm to 200 nm) of polystyrene and polymethacrylate,[14] for evaluating the elastic modulus of amorphous methacrylate films with thickness varying from 10 nm to 40 nm,[15] and evaluating mechanical moduli of organic electronic materials.[16]

We recently introduced a novel *in situ* approach for estimating mechanical properties of luminescent silicon nanocrystals (SiNCs) deposited on flexible substrates made from polydimethylsiloxane (PDMS). In this method, we applied finite bending to the bilayered system of SiNCs/PDMS and noted the angle at which we observed the onset of instabilities.[17] Coupled with theoretical modeling, this critical angle is an indicator of the mechanical properties of the SiNC layers. Our study revealed a neo-Hookean coefficient (μ_0^{NC}, analogous to shear modulus at low stress/strain) of a 4.5 μm thick SiNC film to be 345 ± 23 kPa when deposited on a PDMS substrate with $\mu_0^{P} = 190$ kPa. In that demonstration, we kept SiNC layer properties consistent as a control – however, there are many parameters that could influence the mechanical behavior of the SiNC layers on PDMS. These include layer thickness, surface functionality, and the mechanical properties of the PDMS substrate as a cross-linked material.[18–21] In order to reveal some of these interrelationships, we investigated a set of parameters regarding their influence over the mechanical properties of SiNC layers on PDMS, as evaluated using the same finite bending method. Our results indicate that the layer of SiNCs and PDMS parameters

Department of Mechanical Engineering, Michigan State University, East Lansing, MI, USA. E-mail: ranthony@egr.msu.edu; Fax: +1-517-353-1750; Tel: +1-517-432-7491

† Electronic supplementary information (ESI) available: FTIR of surface-functionalized and bare SiNCs; film thicknesses on PDMS substrates with varying α. See DOI: 10.1039/d0ra06321e

‡ These authors contributed equally to this work.

exert competing influences on the mechanical properties of the SiNC layers. Unraveling the connection of these parameters on the physical, mechanical, and optical properties of the SiNCs will allow advancement for predictive engineering of nanomaterial thin films, for stretchable and flexible devices.

2 Methods

2.1 PDMS sample preparation

We prepared PDMS using a Sylgard prepolymer PDMS 184-kit and curing agent catalyst (Dow Corning). The mechanical properties of the PDMS depend on the mass ratio of the prepolymer and curing agent (α), as well as the curing conditions during PDMS preparation. We produced a range of substrates with identical geometrical dimensions (defined earlier as slenderness ratio in 17). For all experiments performed in this paper, the slenderness ratio of the sample was kept constant at 3. For all experiments that probed the influence of the SiNC layer properties on the SiNC modulus, we held α constant at 10.

We then altered this ratio to produce PDMS samples with lower moduli. Since α varies linearly with the elastic modulus of the PDMS, decreasing the mass fraction of curing agent (*i.e.* increasing the value of α) decreases the modulus of the PDMS.[22] Specifically, for this study we have used PDMS with $\alpha = 10$, 12, and 20. Our estimation method prohibited use of $\alpha < 10$, *i.e.* higher modulus, as the samples ruptured during our testing protocol.

2.2 Uniaxial tensile testing

We performed a standard uniaxial tensile test, using a custom-built test setup, to evaluate the neo-Hookean coefficients of the PDMS. A minimum of 3 samples were taken for each type of sample ($\alpha = 10$, 12, and 20), and an average of the resulting mechanical properties was recorded. Each sample was cut in the shape of a rectangle and mounted on our uniaxial tensile test machine. Four black dots were applied on the surface of the PDMS as fiducial markers, and the sample was stretched between two clamps. One of the clamps had a load cell attached to it to measure the force required for the deformation.

The force from the load cell was converted to Cauchy stress by calculating the average cross-section area of the sample in the loaded configuration. The sample was stretched cyclically for 5 cycles from the reference configuration until a 20% deformation was achieved. A Hitachi KP-M2AN CCD camera was used to capture and feed the image of the fiducial markers during uniaxial stretch into LabVIEW. The test was performed under quasi-static conditions with a strain rate of 0.1 mm s^{-1}. Finally, the Cauchy stress and stretch throughout the test were calculated, and the best fit neo-Hookean modulus was estimated by minimizing the differences between experimental and theoretical stresses at each value of stretch (Table 1).

Table 1 Neo-Hookean coefficients of PDMS for different ratio of base to curing agent, α. Increasing the amount of base while keeping the same amount of curing agent can significantly decrease the mechanical modulus of PDMS

Ratio of base to curing agent, α	Neo-Hookean coefficient [kPa]
10	191.9 ± 34.9
12	112.9 ± 43.4
20	69.8 ± 7.6

2.3 SiNC layer deposition

We synthesized SiNCs using a low-pressure non-thermal radio frequency (RF) plasma as previously described.[17,23,24] The nanocrystals were deposited on the PDMS as thin-film layers by inertial impaction onto a substrate placed beneath a slit-shaped orifice.[25–27] The stand-off distance between orifice outlet and the top surface of PDMS substrate was kept constant at ~4–5 mm to ensure consistency with our prior work.[17,25,26] We rastered the PDMS substrates beneath the orifice to achieve uniform film deposition.

We were interested in the influence of film thickness on SiNC film properties, so we decreased the deposition time from 20 min, as considered in our previous study,[17] to 10 min and 5 min for thinner films, and increased it to 30 min for thicker films. We monitored the frequency of the rastering motion for the substrate (3 s for each back and forth motion) during deposition, to ensure a consistent protocol. We used SEM imaging of scored and FIB-milled samples to measure the SiNC layer thicknesses. Fig. 1 shows the linear dependence of SiNC film thickness on deposition time, without other significant changes in surface or cross-sectional morphology. The film thicknesses are also presented in numerical form in Table 2. Example SEM images are included in the ESI Fig. S-1(a) and (b).†

2.4 In-flight surface functionalization of SiNCs

Surface functionalization of SiNCs with various ligands has been shown to improve their photoluminescence (PL) properties.[27–32] We performed in-flight plasma-initiated surface

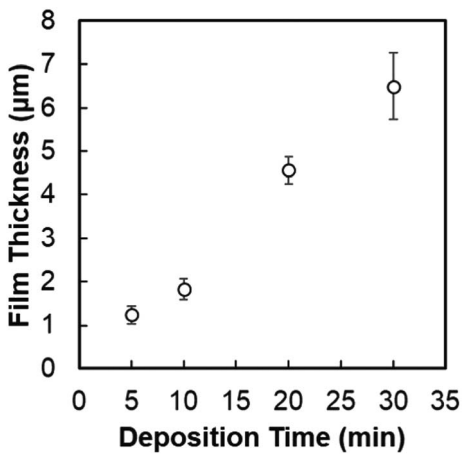

Fig. 1 We performed SEM imaging of film cross-sections to estimate film thickness as a function of deposition time (error bars reflect std deviation).

Table 2 Tabulated values of film thicknesses *vs.* deposition time, as measured using SEM imaging of film cross-sections

Time (min)	Thickness (μm)
5	1.24 ± 0.20
10	1.84 ± 0.23
20	4.56 ± 0.31
30	6.50 ± 0.76

functionalization, following what was described previously.[27] 1-Dodecene vapor is flown into the effluent of the plasma reactor *via* a side-arm injection from a liquid bubbler, carried by H_2 gas to aid with surface defect mitigation.[33] This method for surface functionalization of the SiNCs in the gas phase immediately following their synthesis, in-flight, allows partial surface capping with alkyl chains without solution-phase initiation. We confirmed the reaction using Fourier-transform infrared spectroscopy (FTIR) (see ESI Fig. S-2†).

2.5 Mechanical properties of SiNC layers

For evaluating the mechanical properties of the thin film SiNC deposited on PDMS, we performed mathematical analysis and experiments according to the method we reported previously.[17,34] In short, we adhered the edges of each PDMS slab between two aluminum handles and performed the SiNC deposition onto the PDMS. We conducted finite bending experiments on the bilayers by flexing the aluminum handles to measure the angle for which we observe the onset of bifurcations on the surface of the SiNC layer. This in turn allowed us to estimate the mechanical parameters given the geometry of the sample. The ESI includes a photograph of our apparatus in Fig. S-1(c).† During experiments, the onset of bifurcations was detected by direct visual inspection, and photographs were taken of the profile of the sample to measure the critical angle of bifurcation. Three measurements were taken for each of the samples to ensure accuracy and reproducibility. The bending angle at which bifurcations are first observed is defined as the critical angle of bifurcation. These results were subsequently compared with numerical analyses that predict the angles of bifurcation for bilayers undergoing a finite bending deformation starting from a rectangular cross section.

3 Results and discussion

The neo-Hookean coefficients for the three cases we studied are plotted in Fig. 2, as compared to the standard case from ref. 17. The asterisks on the bars indicate sample conditions which had a statistically significant deviation from the value we obtained for the samples originally examined and reported in ref. 17. Each case is discussed below.

3.1 Influence of film thickness

The numerical model relies on the thickness ratio t between the PDMS thickness and the SiNC layer thickness to evaluate the relationship between the critical angle of bifurcation and the ratio of neo-Hookean coefficients (μ_{ratio}) of the two materials. We deposited SiNC films for varying durations, changing the film thicknesses linearly as shown in Fig. 1, and thus adjusting t. Fig. 3 presents our results on the relation between the critical angle θ_{cr} and μ_{ratio}, depending on t. The lines represent the numerical solution. For each line we have included a shaded region corresponding to a variation of one standard deviation from the average value of t measured. Experimental data points are plotted as symbols.

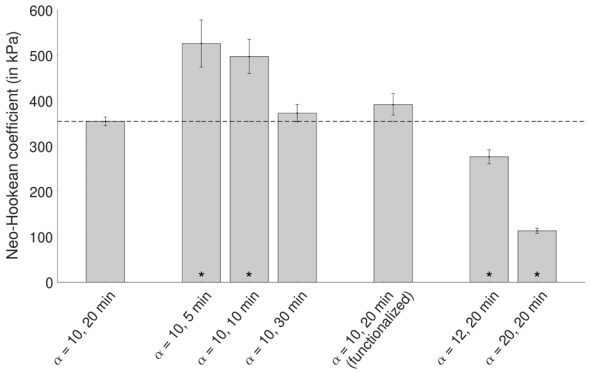

Fig. 2 Neo-Hookean coefficient of all samples. The samples with asterisks indicate sample conditions that led to neo-Hookean coefficients that deviated with statistical significance from samples reported in ref. 17 ($\alpha = 10$, $t = 460$).

Our experimental results yielded t values of 275 ± 36, 460 ± 54, 1100 ± 140, and 1800 ± 351 (with t increasing as deposition time decreases). Note that the results from our numerical model predict that there should be little difference in the relationship between θ_{cr} and μ_{ratio} for the lower two values of t, as shown by the nearly-overlapping curves in Fig. 3. Our experimental results agree well with this prediction, as we did not observe any change in θ_{cr} for samples deposited for 20 and 30 minutes (t = 460 and 275, respectively) despite a clear increase in SiNC layer thickness.

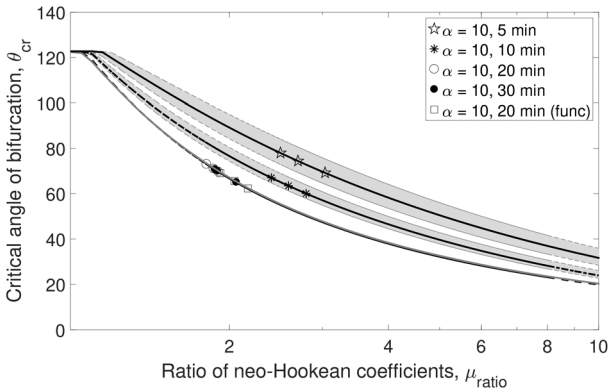

Fig. 3 The methodology introduced in Sinha *et al.*, 2019,[17] employed to estimate neo-Hookean coefficient for SiNC layers corresponding to parametric variation. The lines represent the numerical solution for the average of thickness ratios (t) for a given sample deposition time, and the symbols represent experimental data points. The shaded region shows an area of one standard deviation of the thickness ratio from average for the samples.

For $t > 460$, however, there was a pronounced change in the neo-Hookean coefficient μ_0^{NC}. Increasing t represents a decrease in the thickness of the SiNC layer, and our results show that thinner layers exhibited higher μ_0^{NC} as compared to the thicker layers. Interestingly, for $t = 1100$ and 1800, the samples exhibited μ_0^{NC} values that did not differ statistically from each other, although they did differ from μ_0^{NC} of the thicker SiNC layers. A possible explanation for this observation is that the soft PDMS substrate creates microstructural changes or densifications of the SiNCs, altering their mechanical behavior close to the substrate. Once the layer reaches a certain critical thickness, the effect diminishes as the subsequent layers response to the substrate's mechanical properties decreases with increasing thickness.

3.2 Influence of α

In the base scenario, we used PDMS fabricated with $\alpha = 10$. To investigate the effect of the PDMS modulus on the μ_0^{NC} of the SiNC layers, we also created samples of PDMS with $\alpha = 12$ and 20. As previously noted, an increase in the value of α generates a decrease in the value of μ_0^{P}. Using the protocol mentioned in Section 2.2, the average neo-Hookean coefficients of PDMS with $\alpha = 10$, 12, and 20, were evaluated to be 191.9 $\pm$ 34.9 kPa, 112.9 $\pm$ 43.4 kPa and 69.8 $\pm$ 7.6 kPa respectively. We can clearly see that changing the value of α can significantly affect the material behavior of the PDMS. Concretely, we can determine that increasing the value of α leads to a decrease in the neo-Hookean coefficient for the PDMS. In other words, decreasing the amount of curing agent for the same amount of pre-polymer yields PDMS with a decreased stiffness.

The time of SiNC deposition was kept constant at 20 minutes for all samples, as was the PDMS thickness, and so for all samples for which we changed α, t was ~460. The ESI† contains the table of film thicknesses for SiNC layers deposited on PDMS with varying α. We found that when we reduced μ_0^{P}, the shear modulus of the SiNC layer μ_0^{NC} was also reduced. One explanation for this behavior could be the fact that changing the stiffness of the PDMS by changing α influences the SiNC impaction characteristics, including NC bouncing and adhesion with the substrate and with previously-deposited SiNCs.[35] There are many effects that influence the layer formation during inertial impaction, including the surface roughness of the substrate, the surface adhesion energy, whether the nanoparticles are impinging as individuals or as agglomerates, and more.[35–38] We cannot be sure which of these effects is the most prominent here, but our observations regarding the modification in the shear modulus of the SiNC layer as they relate to α are repeatable. We will investigate this phenomenon in more detail in a future manuscript.

3.3 Influence of surface functionalization

Surface functionalization of SiNCs is typically performed in order to prevent environmental oxidation of the SiNCs by capping surface defects and sterically hindering any surface oxidation effects, and to increase the PL emission intensity and quantum yield of the SiNCs.[28–31] We recently published our research on the differences in neo-Hookean coefficient for nanocomposites of SiNCs and PDMS, based on surface functionality.[39] We found that the surface-functionalized SiNCs in the composite did decrease the neo-Hookean coefficient, but not as dramatically as the bare SiNCs. Because we saw a change in the mechanical behavior of the SiNCs and the surrounding PDMS dependent on surface functionality, we expected to see an effect of functionalization on the mechanical properties of the thin SiNC layers. We hypothesized that the SiNC surfaces (bare or functionalized with alkyl chains) would alter their interactions with one another, causing a change in the mechanical behavior of the layer. For these samples the thickness of the nanocrystal layer was very close to the thickness estimated for the sample with non-functionalized SiNCs for the same deposition time (*i.e.*, 20 min).

Counter to our hypothesis, we found that the critical angle of bifurcation did not differ between layers surface-functionalized and non-functionalized SiNCs (see Fig. 2). This means that the resulting values of μ_0^{NC} were not affected by the functionalization. Despite our findings for the nanocomposites, our results here suggest that the functionalization does not change, mechanically, the particle-to-particle interaction.[39] We intend to continue to probe the dependence of the neo-Hookean coefficient based on the SiNC surface for ultra-thin layers, but as a direct comparison to the standard sample, we observed no difference.

4 Conclusions

In summary, we have investigated the variation of neo-Hookean coefficient μ_0 of SiNC layers deposited directly onto PDMS, as a function of layer thickness, PDMS modulus, and SiNC surface functionality. We discovered that reducing the thickness of the SiNC layer increases the modulus of the layer, consistent with other findings on the modulus of thin films. However, reducing the PDMS modulus by altering the recipe for fabrication causes a significant reduction in the modulus of the SiNC layer. This topic will be the subject of future research, as there are many possible causes for this behavior. Surprisingly, we found that in-flight surface modification does not appear to significantly alter the modulus of the SiNCs. This implies that using in-flight surface modification as a strategy to improve the optical properties of the SiNCs has little impact on the resulting mechanical properties of the SiNC layers. Our ongoing work will continue to investigate the SiNC modulus for much thinner layers, in an effort to understand more intimately the relationship between substrate mechanical properties and the modulus of the deposited SiNCs.

Conflicts of interest

There are no conflicts to declare.

Acknowledgements

This work is funded by the NSF through CMMI Grant #1561964. We gratefully acknowledge Dr Per Askeland for his assistance with FIB milling and SEM.

Notes and references

1 A. Lockwood and B. Inkson, *J. Phys. D: Appl. Phys.*, 2008, **42**, 035410.
2 A. J. Wagner, E. D. Hintsala, P. Kumar, W. W. Gerberich and K. A. Mkhoyan, *Acta Mater.*, 2015, **100**, 256–265.
3 D. Chrobak, N. Tymiak, A. Beaber, O. Ugurlu, W. W. Gerberich and R. Nowak, *Nat. Nanotechnol.*, 2011, **6**, 480–484.
4 B. X. Han, K. Zheng, Y. Zhang, X. Zhang, Z. Zhang and Z. L. Wang, *Adv. Mater.*, 2007, 2112–2118.
5 M. D. Uchic, D. M. Dimiduk, J. N. Florando and W. D. Nix, *Science*, 2004, **305**, 986–989.
6 J. Wang, Z. Zeng, C. R. Weinberger, Z. Zhang, T. Zhu and S. X. Mao, *Nat. Mater.*, 2015, **14**, 594–600.
7 L. Wang, J. Teng, X. Sha, J. Zou, Z. Zhang and X. Han, *Nano Lett.*, 2017, **17**(8), 4733–4739.
8 L. Wang, P. Guan, J. Teng, P. Liu, D. Chen, W. Xie, D. Kong, S. Zhang, T. Zhu, Z. Zhang, E. Ma, M. Chen and X. Han, *Nat. Commun.*, 2017, **8**, 1–7.
9 J. R. Greer, W. C. Oliver and W. D. Nix, *Acta Mater.*, 2005, **53**, 1821–1830.
10 Y. Yue, P. Liu, Z. Zhang and X. Han, *Nano Lett.*, 2011, 3151–3155.
11 J. R. Greer, W. C. Oliver and W. D. Nix, *Acta Mater.*, 2005, **53**, 1821–1830.
12 J. Gaspar, O. Paul, V. Chu and J. Conde, *J. Micromech. Microeng.*, 2010, **20**, 035022.
13 M. D. Uchic, D. M. Dimiduk and J. N. Florando, *Science*, 2004, **305**, 986–990.
14 C. M. Stafford, B. D. Vogt, C. Harrison, D. Julthongpiput and R. Huang, *Macromolecules*, 2006, **39**, 5095–5099.
15 J. M. Torres, C. M. Stafford and B. D. Vogt, *ACS Nano*, 2009, **3**, 2677–2685.
16 D. Tahk, H. H. Lee and D.-Y. Khang, *Macromolecules*, 2009, **42**, 7079–7083.
17 M. Sinha, A. Izadi, R. J. Anthony and S. Roccabianca, *Nanoscale*, 2019, **11**(15), 7520–7526.
18 H. Mohammadi, A. Bahrololoumi, Y. Chen and R. Dargazany, in *Constitutive Models for Rubber XI*, ed. B. Huneau, J.-B. Le Cam, Y. Marco and E. Verron, CRC Press, 1st edn, 2019, pp. 542–547.
19 A. Bahrololoumi and R. Dargazany, *Mechanics of Solids, Structures, and Fluids*, Salt Lake City, Utah, USA, 2019, vol. 9, p. V009T11A029.
20 A. Bahrololoumi, V. Morovati, E. A. Poshtan and R. Dargazany, *Int. J. Plast.*, 2020, **130**, 102676.
21 A. Ghaderi, V. Morovati and R. Dargazany, 2020, arXiv preprint arXiv:2007.03067.
22 I. Johnston, D. McCluskey, C. Tan and M. Tracey, *J. Micromech. Microeng.*, 2014, **24**, 035017.
23 L. Mangolini, E. Thimsen and U. Kortshagen, *Nano Lett.*, 2005, **5**, 655–659.
24 R. Mandal and R. J. Anthony, *ACS Appl. Mater. Interfaces*, 2016, **8**, 35479–35484.
25 Z. C. Holman and U. R. Kortshagen, *Nanotechnology*, 2010, **21**(33), 335302.
26 G. Nava, F. Fumagalli, S. Neutzner and F. Di Fonzo, *Nanotechnology*, 2018, **29**, 465603.
27 R. J. Anthony, K. Y. Cheng, Z. C. Holman, R. J. Holmes and U. R. Kortshagen, *Nano Lett.*, 2012, **12**, 2822–2825.
28 L. Mangolini, D. Jurbergs, E. Rogojina and U. Kortshagen, *J. Lumin.*, 2006, **121**, 327–334.
29 L. Mangolini and U. Kortshagen, *Adv. Mater.*, 2007, **19**, 2513–2519.
30 F. Sangghaleh, I. Sychugov, Z. Yang, J. G. C. Veinot and J. Linnros, *ACS Nano*, 2015, **9**(7), 7097–7104.
31 J. A. Kelly and J. G. C. Veinot, *ACS Nano*, 2010, **4**, 4645–4656.
32 B. N. Jariwala, O. S. Dewey, P. Stradins, C. V. Ciobanu and S. Agarwal, *ACS Appl. Mater. Interfaces*, 2011, **3**, 3033–3041.
33 R. J. Anthony, D. J. Rowe, M. Stein, J. Yang and U. Kortshagen, *Adv. Funct. Mater.*, 2011, **21**, 4041.
34 S. Roccabianca, D. Bigoni and M. Gei, *J. Mech. Mater. Struct.*, 2011, **6**, 511–527.
35 M. Gensch and A. P. Weber, *Adv. Powder Technol.*, 2017, **28**, 1930–1942.
36 A. Alizadeh, V. Bahadur, W. Shang, Y. Zhu, D. Buckley, A. Dhinojwala and M. Sohal, *Langmuir*, 2013, **29**, 4520–4524.
37 I. G. Kavouras and P. Koutrakis, *Aerosol Sci. Technol.*, 2001, **34**, 46–56.
38 W. John, *Aerosol Sci. Technol.*, 1995, **23**, 2–24.
39 A. Izadi, B. Toback, M. Sinha, A. Millar, M. Bigelow, S. Roccabianca and R. Anthony, *Phys. Status Solidi A*, 2020, 2000015.